High-energy properties of the high-redshift flat spectrum radio quasar PKS 2149−306

F. D'Ammando[1,2]⋆ and M. Orienti[2]

[1]*Dip. di Fisica e Astronomia, Università di Bologna, Viale Berti Pichat 6/2, I-40127 Bologna, Italy*
[2]*INAF – Istituto di Radioastronomia, Via Gobetti 101, I-40129 Bologna, Italy*

ABSTRACT

We investigate the γ-ray and X-ray properties of the flat spectrum radio quasar PKS 2149−306 at redshift $z = 2.345$. A strong γ-ray flare from this source was detected by the Large Area Telescope on board the *Fermi Gamma-ray Space Telescope* satellite in 2013 January, reaching on January 20 a daily peak flux of $(301 \pm 36) \times 10^{-8}$ ph cm^{-2} s^{-1} in the 0.1–100 GeV energy range. This flux corresponds to an apparent isotropic luminosity of $(1.5 \pm 0.2) \times 10^{50}$ erg s^{-1}, comparable to the highest values observed by a blazar so far. During the flare the increase of flux was accompanied by a significant change of the spectral properties. Moreover significant flux variations on a 6-h time-scale were observed, compatible with the light crossing time of the event horizon of the central black hole. The broad-band X-ray spectra of PKS 2149−306 observed by *Swift-XRT* and *NuSTAR* are well described by a broken power-law model, with a very hard spectrum ($\Gamma_1 \sim 1$) below the break energy, at $E_{break} = 2.5$–3.0 keV, and $\Gamma_2 \sim$ 1.4–1.5 above the break energy. The steepening of the spectrum below ~ 3 keV may indicate that the soft X-ray emission is produced by the low-energy relativistic electrons. This is in agreement with the small variability amplitude and the lack of spectral changes in that part of the X-ray spectrum observed between the two *NuSTAR* and *Swift* joint observations. As for the other high-redshift FSRQ detected by both *Fermi-LAT* and *Swift-BAT*, the photon index of PKS 2149−306 in hard X-ray is 1.6 or lower and the average γ-ray luminosity higher than 2 $\times 10^{48}$ erg s^{-1}.

Key words: galaxies: active – quasars: individual: PKS 2149−306 – quasars: general – gamma-rays: galaxies – gamma-rays: general – X-rays: galaxies.

1 INTRODUCTION

Blazars are radio-loud active galactic nuclei (AGN), with powerful relativistic jets observed at a small viewing angle. For this reason their emission is strongly enhanced due to Doppler boosting and they are expected to be detected up to high redshift. The most distant blazar identified so far is Q0906+6930 (Romani et al. 2004), located at redshift $z = 5.47$. A possible excess of γ-ray photons from a position compatible with this flat spectrum radio quasar (FSRQ) was observed by EGRET (Romani 2006), but has not been confirmed by *Fermi Large Area Telescope* (*LAT*) observations so far. Recently, two FSRQ at redshift $z > 5$, B2 1023+25 and SDSS J114657.79+403708.6, were detected in hard X-rays by *NuSTAR* and identified as blazars (Sbarrato et al. 2013; Ghisellini et al. 2014a). Both objects have never been detected in γ rays. The most distant FSRQ reported in the Third *Fermi-LAT* catalogue (3FGL;

Acero et al. 2015) is PKS 0537−286 at redshift $z = 3.104$, indicating the difficulty in detecting quasars at $z > 3$ in the γ-ray regime.

PKS 2149−306 (RA $= 21^{h}51^{m}55^{s}\!.5239$, Dec. $= -30°27'53''\!.697$, J2000; Johnston et al. 1995) is an FSRQ at redshift $z = 2.345$ (Wilkes 1986). The source is bright in X-rays, showing substantial variability both in intensity and spectral slope, as indicated by *ROSAT* (Siebert et al. 1996), *ASCA* (Cappi et al. 1997), *XMM–Newton* (Ferrero & Brinkmann 2003), and *Swift* observations (Sambruna et al. 2007; Bianchin et al. 2009). A tentative detection of an emission line at ~ 17 keV in the source frame by *ASCA* was interpreted as highly blueshifted Fe Kα (Yaqoob et al. 1999). This finding was not confirmed by Fang et al. (2001) and Page et al. (2004) using *Chandra* data. As for other FSRQ, a low-energy photon deficit in X-rays was suggested for PKS 2149−306, possibly due to an absorbing cloud in the source rest frame (e.g. Sambruna et al. 2007) or to a low-energy tail of the electron population (e.g. Tavecchio et al. 2007). PKS 2149−306 was detected in hard X-rays with a hard spectrum by *Beppo*SAX (Elvis et al. 2000), *Swift-BAT* (Baumgartner et al. 2013), *INTEGRAL*-IBIS (Beckmann et al. 2009), and lately *NuSTAR* (Tagliaferri et al. 2015).

⋆E-mail: dammando@ira.inaf.it

Table 1. Unbinned likelihood spectral fit results.

Date (UT)	Date (MJD)	PL		LP			
		Γ	TS_{PL}	α	β	TS_{LP}	TS_{Curve}
2008 Aug 04/2014 Aug 04	54682–56873	2.79 ± 0.03	2096	2.36 ± 0.05	0.29 ± 0.03	2183	87
2011 Feb 03/2011 Mar 05	55595–55625	2.85 ± 0.08	521	2.53 ± 0.13	0.28 ± 0.09	538	18
2013 Jan 04/2013 Feb 02	56296–56325	2.45 ± 0.05	1239	1.99 ± 0.11	0.28 ± 0.06	1273	34

Among the high-redshift ($z > 2$) blazars, 64 were reported in the 3FGL (Acero et al. 2015). Only two of these objects are at redshift $z > 3$. In contrast, 10 blazars at redshift $z > 3$ were detected in hard X-rays by *Swift-BAT* (Baumgartner et al. 2013), *INTEGRAL*-IBIS (Bassani et al. 2012), and *NuSTAR* (Sbarrato et al. 2013; Ghisellini et al. 2014a). In particular, seven blazars at redshift $z > 3$ are detected by *Swift-BAT*. Therefore, observations in the hard X-ray band seem to be more effective than the γ-ray band for finding blazars at redshift $z > 3$. This might be due to the fact that high-redshift blazars generally have the inverse Compton (IC) peak at hundreds of keV and thus are not ideal for a detection at GeV energies (e.g. Ghisellini et al. 2011; Ghisellini 2013). For this reason, the detection of a γ-ray flare from a high-redshift blazar may be even more interesting with respect to the flaring activity from other blazars.

On 2013 January 4, a strong γ-ray flare from PKS 2149−306 was detected by *Fermi-LAT* (preliminary results were reported in D'Ammando & Orienti 2012). The aim of this paper is to discuss the γ-ray and X-ray properties of this source and to make a comparison with the other high-redshift blazars detected by *Fermi-LAT* and *Swift-BAT* using the 3FGL catalogue (Acero et al. 2015) and the 70-month *Swift-BAT* catalogue (Baumgartner et al. 2013).

This paper is organized as follows. In Section 2, we report the *LAT* data analysis and results, while in Sections 3, 4, and 5 we present the results of the *Swift*, *XMM–Newton*, and *NuSTAR* observations, respectively. We discuss the properties of the source in Section 6, while in Section 7 we summarize our results. Throughout the paper, a Λ cold dark matter cosmology with $H_0 = 71$ km s^{-1} Mpc^{-1}, $\Omega_\Lambda = 0.73$, and $\Omega_m = 0.27$ is adopted (Komatsu et al. 2011). The corresponding luminosity distance at $z = 2.345$ (i.e. the source redshift) is $d_L = 19240$ Mpc. Throughout this paper the quoted uncertainties are given at 1σ level, unless otherwise stated. For power-law (PL) spectra $dN/dE \propto E^{-\Gamma_{X,\gamma}}$ we denote as Γ_X and Γ_γ the spectral indices in the X-ray and γ-ray bands, respectively.

2 *FERMI-LAT* DATA: SELECTION AND ANALYSIS

The *Fermi-LAT* is a pair-conversion telescope operating from 20 MeV to more than 300 GeV. It has a large peak effective area (~8000 cm^2 for 1 GeV photons), and a field of view of about 2.4 sr with an angular resolution (68 per cent containment angle) of 0°.6 for a single photon at $E = 1$ GeV on-axis. Details about the *Fermi-LAT* are given in Atwood et al. (2009).

The *LAT* data reported in this paper were collected from 2008 August 4 (MJD 54682) to 2014 August 4 (MJD 56873). During this period, the *LAT* instrument operated almost entirely in survey mode. The analysis was performed with the SCIENCETOOLS software package version v9r33p0.[1] Only events belonging to the 'Source' class were used. In addition, a cut on the zenith angle (<100°) was applied to reduce contamination from the Earth limb γ rays,

which are produced by cosmic rays interacting with the upper atmosphere. The spectral analysis was performed with the instrument response functions P7REP_SOURCE_V15 using an unbinned maximum-likelihood method implemented in the Science tool gt-like. Isotropic ('iso_source_v05.txt') and Galactic diffuse emission ('gll_iem_v05_rev1.fit') components were used to model the background.[2] The normalizations of both components were allowed to vary freely during the spectral fittings.

We analysed a region of interest of 10° radius centred at the location of PKS 2149−306. We evaluated the significance of the γ-ray signal from the source by means of a maximum-likelihood test statistic, TS = $2 \times (\log L_1 - \log L_0)$, where L is the likelihood of the data given the model with (L_1) or without (L_0) a point source at the position of PKS 2149−306 (e.g. Mattox et al. 1996). The source model used in gtlike includes all the point sources from the 3FGL catalogue that fall within 15° of PKS 2149−306. The spectra of these sources were parametrized by a PL, a log parabola (LP), or a super exponential cut-off, as in the 3FGL catalogue. A first maximum-likelihood analysis was performed to remove from the model the sources having TS < 10 and/or the predicted number of counts based on the fitted model $N_{pred} < 1$. A second maximum-likelihood analysis was performed on the updated source model. In the fitting procedure, the normalization factors and the spectral shape parameters of the sources lying within 10° of PKS 2149−306 were left as free parameters. For the sources located between 10° and 15° from our target, we kept the normalization and the spectral shape parameters fixed to the values from the 3FGL catalogue.

Integrating over the period 2008 August 4–2014 August 4 (MJD 54682–56873) using a PL model, $dN/dE \propto (E/E_0)^{-\Gamma}$, the fit results in TS = 2096 in the 0.1–100 GeV energy range, and a photon index $\Gamma_\gamma = 2.79 \pm 0.03$. The average flux is $(10.6 \pm 0.4) \times 10^{-8}$ ph cm^{-2} s^{-1}. In order to test for curvature in the γ-ray spectrum of PKS 2149−306 an alternative spectral model to a PL, an LP, $dN/dE \propto (E/E_0)^{-\alpha - \beta \log(E/E_0)}$, was used for the fit. We obtain a spectral slope $\alpha = 2.36 \pm 0.05$ at the reference energy $E_0 = 221$ MeV, a curvature parameter around the peak $\beta = 0.29 \pm 0.03$, with TS = 2183 and an average flux of $(9.7 \pm 0.4) \times 10^{-8}$ ph cm^{-2} s^{-1} (Table 1). We used a likelihood ratio test (LRT) to check the PL model (null hypothesis) against the LP model (alternative hypothesis). Following Nolan et al. (2012), these values may be compared by defining the curvature test statistic $TS_{curve} = TS_{LP} - TS_{PL}$, which in this case results in $TS_{curve} = 87$ (~9.3σ), meaning that we have evidence of significant curvature in the average γ-ray spectrum.

Fig. 1 shows the γ-ray light curve for the first six years of *Fermi-LAT* observations of PKS 2149−306 using an LP model and 1-month time bins. For each time bin, the spectral shape parameters of PKS 2149−306 and all sources within 10° of it were frozen to the values resulting from the likelihood analysis over the entire period. If TS < 10, 2σ upper limits were calculated. The statistical

---

[1] http://fermi.gsfc.nasa.gov/ssc/data/analysis/software/

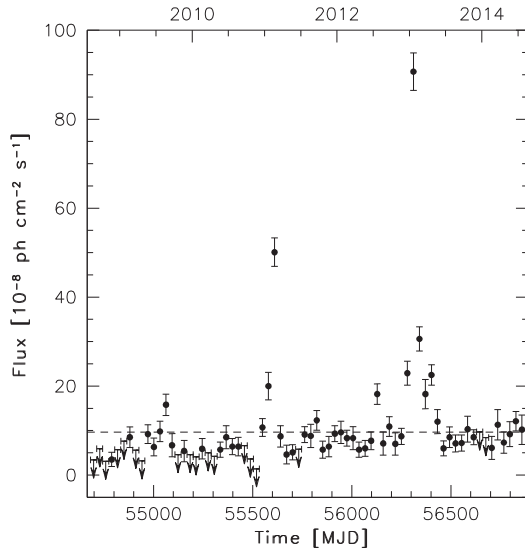[2] http://fermi.gsfc.nasa.gov/ssc/data/access/lat/BackgroundModels.html

Figure 1. Integrated flux light curve of PKS 2149−306 obtained by *Fermi-LAT* in the 0.1–100 GeV energy range during 2008 August 4–2014 August 4 (MJD 54682–56873) using an LP model with 30-day time bins. Arrows refer to 2σ upper limits on the source flux. Upper limits are computed when TS < 10. The dashed line represents the mean flux.

uncertainty in the fluxes are larger than the systematic uncertainty (Ackermann et al. 2012) and only the former is considered in the paper.

During the first two years of *Fermi* operation, PKS 2149−306 was observed in a low-activity state, with an average (0.1–100 GeV) flux of $(6.4 \pm 0.6) \times 10^{-8}$ ph cm^{-2} s^{-1} and a spectrum described by an PL model with photon index of $\Gamma_\gamma = 3.00 \pm 0.09$ (Nolan et al. 2012). Different from the average spectrum over six years of observations, no significant curvature of the spectrum was observed during the low-activity period between 2008 August and 2010 July.

This difference may be related to the low statistics in the first two years that may prevent the detection of spectral curvature, as observed for other FSRQ (e.g. PKS 1510−089 and S5 0836+710; Abdo et al. 2010b; Akyuz et al. 2013). Flaring activity from this source was first observed in 2011 February, and subsequently an even stronger flare was detected in 2013 January (Fig. 1).

2.1 Flaring periods

Leaving the spectral shape parameters free to vary during the first high-activity period (2011 February 3–March 5; MJD 55595–55625), using an LP model, the fit results in a spectral slope $\alpha = 2.53 \pm 0.13$ at the reference energy $E_0 = 221$ MeV, a curvature parameter around the peak $\beta = 0.28 \pm 0.09$, with TS = 538 and an average flux of $(51.3 \pm 4.1) \times 10^{-8}$ ph cm^{-2} s^{-1}. Using a PL model, the fit results in TS = 521 and a photon index of $\Gamma_\gamma = 2.85 \pm 0.08$ (Table 1). Using an LRT, we obtain TS$_{\text{curve}}$ = 18 ($\sim 4.2\sigma$), i.e. a significant curvature of the γ-ray spectrum in 2011 February.

During the second high-activity period (2013 January 4–February 2; MJD 56296–56325), using an LP model the fit results in a spectral slope $\alpha = 1.99 \pm 0.11$ at the reference energy $E_0 = 221$ MeV, a curvature parameter around the peak $\beta = 0.28 \pm 0.06$, with TS = 1273 and an average flux of $(77.4 \pm 5.1) \times 10^{-8}$ ph cm^{-2} s^{-1}. Using a PL model the fit results in TS = 1239 and a photon index of $\Gamma_\gamma = 2.45 \pm 0.05$ (Table 1). Using an LRT, we obtain TS$_{\text{curve}}$ = 34 ($\sim 5.8\sigma$), indicating a significant curvature of the γ-ray spectrum in that period.

In the following analysis of the light curves on sub-daily timescales, we fixed the flux of the diffuse emission components at the value obtained by fitting the data over the respective daily time-bins. In Fig. 2, we show a light curve focused on the period 2011 February 3–March 5 (left-hand plot) and 2013 January 4–February 2 (right-hand plot), with 1-day (upper panel), 12-h (middle panel), and 6-h (lower panel) time bins. For each time bin, the spectral shape parameters of PKS 2149−306 and all sources within 10° of
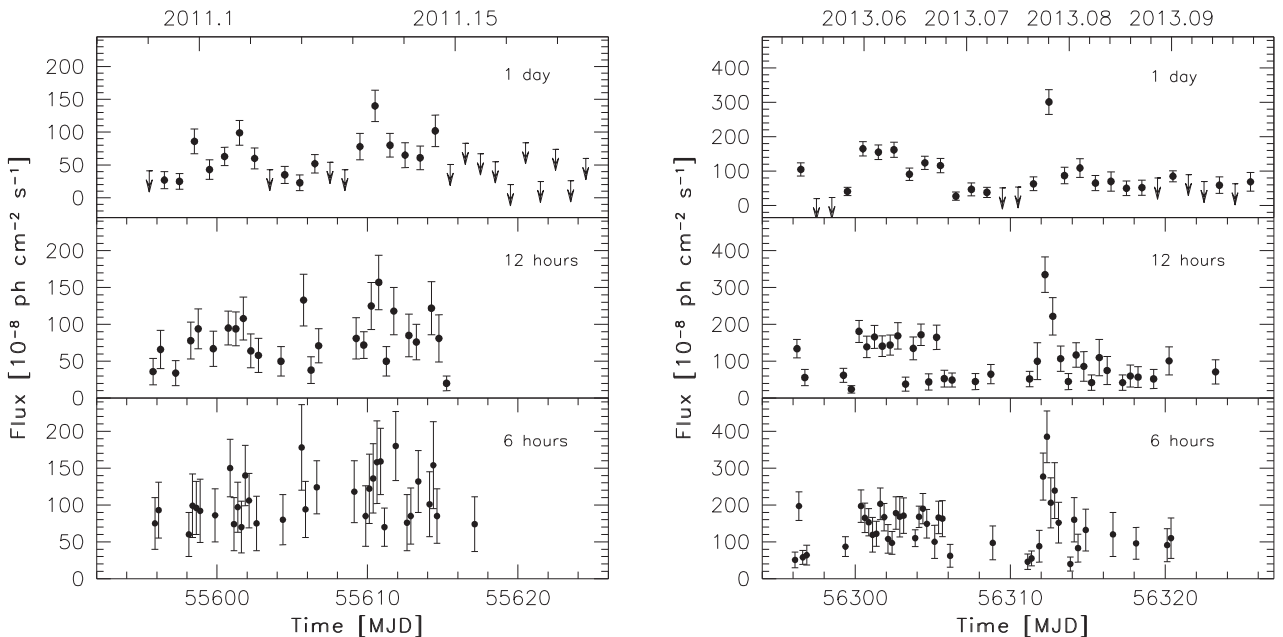

Figure 2. Integrated flux light curve of PKS 2149−306 obtained by *Fermi-LAT* in the 0.1–100 GeV energy range during 2011 February 3–March 5 (left-hand plot) and 2013 January 4–February 2 (right-hand plot), with 1-day time bins (upper panel), 12-h time bins (middle panel), and 6-h time bins (bottom panel). Arrows refer to 2σ upper limits on the source flux. Upper limits are computed when TS < 10. In the middle and bottom panels upper limits are not shown.

Table 2. Log and fitting results of *Swift-XRT* observations of PKS 2149−306 using a PL model with N_H fixed to the Galactic absorption.

Date (UT)	Date (MJD)	Net exposure time (s)	Photon index (Γ_X)	Flux 0.3–10 keV ($\times 10^{-11}$ erg cm^{-2} s^{-1})	χ^2/d.o.f.
2005 Dec 10	53714	3314	1.47 ± 0.08	1.52 ± 0.12	44/45
2005 Dec 13	53717	2255	1.39 ± 0.10	1.69 ± 0.10	32/25
2009 Apr 23	54944	3114	1.23 ± 0.11	1.32 ± 0.07	36/31
2009 Apr 29	54950	1773	1.34 ± 0.14	1.21 ± 0.09	16/16
2009 May 05	54956	2889	1.36 ± 0.10	1.22 ± 0.07	28/28
2009 May 14	54965	2924	1.32 ± 0.08	1.75 ± 0.07	40/41
2009 May 23	54974	2989	1.40 ± 0.11	1.58 ± 0.09	31/28
2009 May 29	54980	2565	1.19 ± 0.08	1.91 ± 0.10	39/36
2010 May 11	55327	4760	1.30 ± 0.08	1.17 ± 0.05	38/44
2011 May 07	55688	2947	1.01 ± 0.09	1.96 ± 0.12	35/38
2011 Nov 10	55875	3261	1.33 ± 0.07	1.87 ± 0.09	39/48
2013 Dec 16/17	56642/43	7956	1.09 ± 0.04	2.80 ± 0.08	143/139
2014 Mar 28	56744	2537	1.13 ± 0.08	2.58 ± 0.11	47/44
2014 Apr 18	56765	6331	1.08 ± 0.05	2.60 ± 0.07	126/106[a]

Note. [a]The model that best fits this observation is a broken PL (see Section 3.2).

it were frozen to the values resulting from the likelihood analysis over the entire period considered.

In 2011, the daily peak of the emission was observed on February 18 (MJD 55610) with a flux of $(140 \pm 24) \times 10^{-8}$ ph cm^{-2} s^{-1} in the 0.1–100 GeV energy range, a factor of about 14 higher than the average flux over six years of *Fermi* observations. The corresponding apparent isotropic γ-ray luminosity peak in the 0.1–100 GeV energy range is $(5.3 \pm 0.9) \times 10^{49}$ erg s^{-1}. On 12-h and 6-h time-scale the observed peak flux is $(157 \pm 37) \times 10^{-8}$ and $(180 \pm 47) \times 10^{-8}$ ph cm^{-2} s^{-1}, corresponding to an apparent isotropic γ-ray luminosity of $(5.9 \pm 1.3) \times 10^{49}$ and $(6.8 \pm 1.7) \times 10^{49}$ erg s^{-1}, respectively.

In 2013, the daily peak of the emission was observed on January 20 (MJD 56312) with a flux of $(301 \pm 36) \times 10^{-8}$ ph cm^{-2} s^{-1} in the 0.1–100 GeV energy range, i.e. a factor of about 30 higher than the average flux over six years of *Fermi* observations. The corresponding apparent isotropic γ-ray luminosity peak in the 0.1–100 GeV energy range is $(1.5 \pm 0.2) \times 10^{50}$ erg s^{-1}. On 12-h and 6-h time-scales the observed peak flux is $(335 \pm 48) \times 10^{-8}$ and $(385 \pm 70) \times 10^{-8}$ ph cm^{-2} s^{-1}, corresponding to an apparent isotropic γ-ray luminosity of $(1.6 \pm 0.2) \times 10^{50}$ and $(1.9 \pm 0.3) \times 10^{50}$ erg s^{-1}, respectively. By means of the gtsrcprob tool, we estimated that during this flare the highest energy photon emitted by PKS 2149−306 (with probability >80 per cent to be associated with the target) was observed on 2013 January 12 with an energy of 4.8 GeV.

3 *SWIFT* DATA: ANALYSIS AND RESULTS

The *Swift* satellite (Gehrels et al. 2004) performed 16 observations of PKS 2149−306 between 2005 December and 2014 April. The observations were performed with all three instruments on board: the *X-ray Telescope* (*XRT*; Burrows et al. 2005, 0.2–10.0 keV), the *Ultraviolet/Optical Telescope* (*UVOT*; Roming et al. 2005, 170–600 nm) and the *Burst Alert Telescope* (*BAT*; Barthelmy et al. 2005, 15–150 keV).

3.1 *Swift-BAT*

The hard X-ray flux of this source is below the sensitivity of the *BAT* instrument for the short exposures of the single observations,

therefore those data from this instrument were not used. On the other hand, the source is included in the *Swift-BAT* 70-month hard X-ray catalogue (Baumgartner et al. 2013). The 14–195 keV spectrum is well described by a PL with photon index of $\Gamma_X = 1.50 \pm 0.10$ (χ^2/d.o.f. = 4.8/6). The resulting 14–195 keV flux is $(8.3 \pm 0.6) \times 10^{-11}$ erg cm^{-2} s^{-1}.

3.2 *Swift-XRT*

The *XRT* data were processed with standard procedures, filtering, and screening criteria by using the xrtpipeline v0.13.0 included in the HEASOFT package (v6.15).[3] The data were collected in photon counting mode for all the observations. The source count rate was low (<0.5 counts s^{-1}); thus pile-up correction was not required. The data collected in observations separated by less than 24 hours (i.e. 2010 May 11, obsid: 31404008 and 31404009; 2011 May 7, obsid: 31404010 and 31404011; 2013 December 16–17, obsid: 31404013 and 31404014) were summed in order to have enough statistics to obtain a good spectral fit. Source events were extracted from a circular region with a radius of 20 pixels (1 pixel ∼2.36 arcsec; Burrows et al. 2005), while background events were extracted from a circular region with radius of 50 pixels far away from bright sources. Ancillary response files were generated with xrtmkarf, and account for different extraction regions, vignetting and point spread function corrections. We used the spectral redistribution matrices in the Calibration data base (CALDB) maintained by HEASARC.[4] The spectra were rebinned with a minimum of 20 counts per energy bin to allow for χ^2 spectrum fitting. Bad channels, including zero-count bins, were ignored in the fit. We have fitted the spectrum using XSPEC[5] with an absorbed PL using the photoelectric absorption model tbabs (Wilms, Allen & McCray 2000), with a neutral hydrogen column density fixed to its Galactic value (1.63×10^{20} cm^{-2}; Kalberla et al. 2005). The results are reported in Table 2. All errors are given at the 90 per cent confidence level. Symmetric errors are reported, obtained by averaging the positive and negative errors calculated with XSPEC.

[3] http://heasarc.nasa.gov/lheasoft/
[4] https://heasarc.gsfc.nasa.gov/
[5] https://heasarc.gsfc.nasa.gov/xanadu/xspec/manual/manual.html

Table 3. Observed magnitudes obtained by *Swift-UVOT* for PKS 2149−306. Upper limits are calculated when the analysis provided a significance of detection <3σ.

Date (UT)	Date (MJD)	v	b	u	$w1$	$m2$	$w2$
2005 Dec 10	53714	17.46 ± 0.14	17.76 ± 0.12	17.15 ± 0.11	17.92 ± 0.14	20.22 ± 0.41	19.79 ± 0.25
2005 Dec 13	53717	17.56 ± 0.21	17.55 ± 0.15	17.02 ± 0.12	18.12 ± 0.19	19.63 ± 0.20	20.16 ± 0.44
2009 Apr 23	54944	17.94 ± 0.23	17.88 ± 0.13	17.30 ± 0.13	18.59 ± 0.22	>19.82	>20.37
2009 Apr 29	54950	17.85 ± 0.23	18.22 ± 0.16	17.85 ± 0.15	18.73 ± 0.27	>19.45	>20.21
2009 May 05	54956	17.32 ± 0.16	17.82 ± 0.13	17.35 ± 0.14	18.52 ± 0.24	>19.69	>20.25
2009 May 14	54965	17.65 ± 0.17	17.99 ± 0.12	17.17 ± 0.12	18.32 ± 0.19	>19.84	>20.44
2009 May 23	54974	17.79 ± 0.16	18.08 ± 0.11	17.34 ± 0.11	18.24 ± 0.16	>20.04	20.20 ± 0.30
2009 May 29	54980	17.82 ± 0.23	17.71 ± 0.11	17.25 ± 0.12	18.42 ± 0.19	>19.54	20.36 ± 0.39
2010 May 11	55327	17.84 ± 0.09	18.25 ± 0.08	17.64 ± 0.08	18.38 ± 0.10	–	–
2011 May 07	55688	17.56 ± 0.07	17.95 ± 0.10	18.12 ± 0.08	–	–	20.12 ± 0.22
2011 Nov 10	55875	17.92 ± 0.09	18.16 ± 0.07	17.63 ± 0.08	–	–	–
2013 Dec 16	56642	17.87 ± 0.16	17.92 ± 0.10	17.22 ± 0.10	18.31 ± 0.14	19.92 ± 0.30	20.24 ± 0.28
2013 Dec 17	56643	17.57 ± 0.18	18.14 ± 0.15	17.23 ± 0.12	18.22 ± 0.18	>19.54	>20.20
2014 Mar 28	56744	17.80 ± 0.20	17.87 ± 0.11	17.24 ± 0.11	18.31 ± 0.17	>19.75	20.35 ± 0.36
2014 Apr 18	56765	17.79 ± 0.17	17.92 ± 0.10	17.24 ± 0.10	18.61 ± 0.17	>20.06	20.34 ± 0.32

For the observations performed on 2013 December 16–17 and 2014 April 18 there is enough statistic for testing a more detailed spectral model with respect to a simple PL. For the 2013 December observations, using a broken PL the fit results in $\Gamma_1 = 0.95^{+0.08}_{-0.13}$ below the break energy $E_{break} = 2.40^{+0.64}_{-0.92}$ keV and $\Gamma_2 = 1.32^{+0.16}_{-0.15}$ above E_{break}. The fit with a broken PL (χ^2/d.o.f = 129/137) does not improve with respect to a simple PL (χ^2/d.o.f = 143/139). For the 2014 April observation using a broken PL the fit results in $\Gamma_1 = 0.97 \pm 0.09$ below the break energy $E_{break} = 2.76^{+1.33}_{-0.81}$ keV and $\Gamma_2 = 1.34^{+0.36}_{-0.17}$ above E_{break} (χ^2/d.o.f = 116/104). The F-test shows an improvement of the fit with respect to the simple PL (χ^2/d.o.f = 126/106) with a probability of 97.9 per cent, indicating that the broken PL is the best-fitting model.

3.3 *Swift-UVOT*

UVOT data in the v, b, u, $w1$, $m2$, and $w2$ filters were analysed with the uvotsource task included in the HEASOFT package (v6.15) and the 20130118 CALDB-UVOTA release. Source counts were extracted from a circular region of 5 arcsec radius centred on the source, while background counts were derived from a circular region with 10 arcsec radius in a nearby, free region. The observed magnitudes are reported in Table 3. Upper limits at 90 per cent confidence level are calculated using the *UVOT* photometric system when the analysis provided a significance of detection <3σ.

4 *XMM–NEWTON*: DATA ANALYSIS AND RESULTS

XMM–Newton (Jansen et al. 2001) observed PKS 2149−306 on 2001 May 1 for a total duration of 25 ks (observation ID 0103060401, PI: Aschenbach). The EPIC pn was operated in the large-window mode and the EPIC MOS cameras (MOS1 and MOS2) were operated in the full-frame mode. The data were reduced using the *XMM–Newton* Science Analysis System (SAS v14.0.0), applying standard event selection and filtering. Inspection of the background light curves showed that no strong flares were present during the observation, with good exposure times of 20, 24 and 24 ks for the pn, MOS1 and MOS2, respectively. For each of the detectors the source spectrum was extracted from a circular re-

Table 4. Summary of fits to the 0.3–10 keV *XMM–Newton* spectrum of PKS 2149−306. Fits also included absorption fixed at the Galactic value. Flux and E_{break} are given in units of erg cm^{-2} s^{-1} and keV, respectively.

Model	Parameter	Value
PL	Γ	1.45 ± 0.01
	Flux (0.3–10 keV)	$(7.9 \pm 0.1) \times 10^{-12}$
	χ^2/d.o.f.	375/428
Broken PL	Γ_1	1.47 ± 0.02
	E_{break}	$2.4^{+1.3}_{-1.1}$
	Γ_2	$1.42^{+0.03}_{-0.07}$
	Flux (0.3–10 keV)	$(7.9 \pm 0.2) \times 10^{-12}$
	χ^2/d.o.f.	369/426

gion of radius 30 arcsec centred on the source, and the background spectrum from a nearby region of radius 30 arcsec on the same chip. All the spectra were binned to contain at least 20 counts per bin to allow for χ^2 spectral fitting.

All spectral fits were performed over the 0.3–10 keV energy range using XSPEC v.12.8.2. The energies of spectral features are quoted in the source rest frame, while plots are in the observer frame. All errors are given at the 90 per cent confidence level. The data from the three EPIC cameras were initially fitted separately, but since good agreement was found (<5 per cent) we proceeded to fit them together. Galactic absorption was included in all fits using the tbabs model. The results of the fits are presented in Table 4. As reported also in Ferrero & Brinkmann (2003) and Bianchin et al. (2009), a simple PL model is sufficient to describe the data, although some residuals are present (Fig. 3). The flux observed by *XMM–Newton* in the 0.3–10 keV energy range is a factor of 2–3 lower than those observed by *Swift-XRT* during 2005–2014.

A broken PL does not improve the fit and the associated uncertainties on photon index and flux are larger than those from a fit with a simple PL (Table 4). In order to check for the presence of intrinsic absorption, a neutral absorber at the redshift of the source was added to this model, but it did not improve the fit quality and thus is not required. Moreover, no Iron line was detected in the spectrum, in agreement with Page et al. (2004). The 90 per cent upper limit on the equivalent width (EW) of a narrow emission line at 6.4 keV is EW < 17 eV.
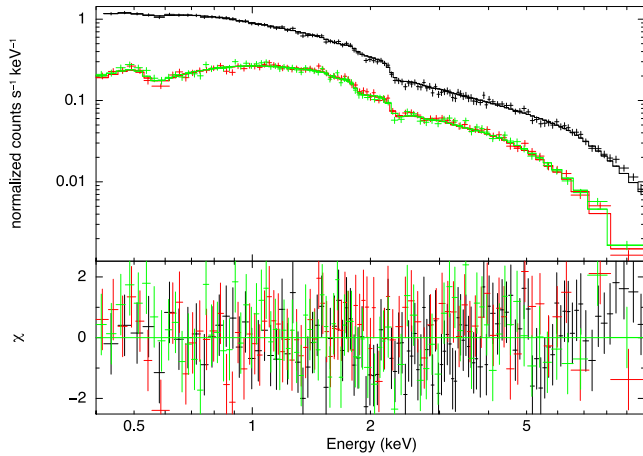
Figure 3. EPIC spectra and residuals of PKS 2149−306 fitted with a PL model.

Table 5. Summary of the results for the fits of the 3.0–76 keV *NuSTAR* spectra collected on 2013 December 17 and 2014 April 18.

Date (UT)	Photon index (Γ_X)	Flux 3.0–76 keV ($\times 10^{-11}$ erg cm^{-2} s^{-1})	χ^2/d.o.f.
2013 Dec 17	1.37 ± 0.01	11.5 ± 0.2	797/805
2014 Apr 18	1.46 ± 0.01	8.2 ± 0.1	735/747

5 *NUSTAR*: DATA ANALYSIS AND RESULTS

NuSTAR (Harrison et al. 2013) observed PKS 2149−306 with its two coaligned X-ray telescopes with corresponding focal planes, focal plane module A (FPMA) and B (FPMB), on 2013 December 17 and on 2014 April 18 for a net exposure time of 38.5 ks and 44.1 ks, respectively. The level 1 data products were processed with the *NuS-TAR* Data Analysis Software (NUSTARDAS) package (v1.4.1). Cleaned event files (level 2 data products) were produced and calibrated using standard filtering criteria with the NUPIPELINE task and version 20140414 of the calibration files available in the *NuSTAR* CALDB. Spectra of the sources were extracted from the cleaned event files using a circle of 20 pixel (49 arcsec) radius, while the background was extracted from two distinct nearby circular regions of 50 pixel radius. The ancillary response files were generated with the numkarf task, applying corrections for the point spread function losses, exposure maps and vignetting. The spectra were rebinned with a minimum of 20 counts per energy bin to allow for χ^2 spectrum fitting. All errors are given at the 90 per cent confidence level.

By fitting the *NuSTAR* spectrum in the 3–76 keV energy range[6] a good fit was obtained using a simple PL for both the observations (χ^2/d.o.f. = 797/805 and 735/747), with photon index $\Gamma_X = 1.37 \pm 0.01$ and $\Gamma_X = 1.46 \pm 0.01$ (Table 5), that is the same value obtained for Γ_2 with a broken PL model over the 0.3–76 keV energy range (see Section 5.1).

5.1 Joint *NuSTAR* and *Swift-XRT* analysis

Simultaneously to *NuSTAR* observations, *Swift-XRT* observations were performed on 2013 December 16–17 and on 2014 April 18.

---

[6] We ignored the zero-variance bins in the spectrum, i.e. the 76–79 keV energy range.

Table 6. Summary of the results for the fits of the 0.3–76 keV *Swift-XRT* and *NuSTAR* spectra collected on 2013 December 16–17 (Obs 1) and 2014 April 18 (Obs 2). All fits also included absorption fixed at the Galactic value.

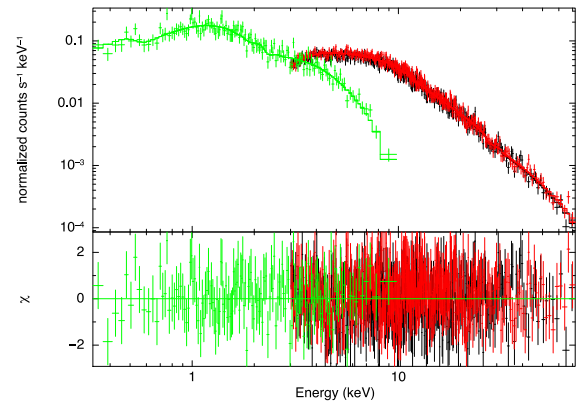| Model	Parameter	Value (Obs 1)	Value (Obs 2)
PL	Γ	1.35 ± 0.01	1.43 ± 0.01
	χ^2/d.o.f.	1013/943	983/851
Broken PL	Γ_1	$0.97^{+0.09}_{-0.07}$	$0.97^{+0.09}_{-0.07}$
	E_{break} (keV)	$2.60^{+0.46}_{-0.56}$	$2.98^{+0.47}_{-0.36}$
	Γ_2	1.37 ± 0.01	1.46 ± 0.01
	χ^2/d.o.f.	924/941	834/849
PL + Extra absorber	Γ	1.36 ± 0.01	1.45 ± 0.01
	N_H^z (cm^{-2})	$1.01^{+0.28}_{-0.24} \times 10^{22}$	$1.36^{+0.39}_{-0.33} \times 10^{22}$
	χ^2/d.o.f.	966/942	895/850

Figure 4. *NuSTAR* (red and black points) and *Swift-XRT* (green points) spectra and residuals of PKS 2149−306 collected on 2013 December 16–17, simultaneously fitted with a broken PL.

This allows us to study the X-ray spectrum of PKS 2149−306 over a wide energy range, i.e. 0.3–76 keV. The results of the simultaneous fits of the *NuSTAR* and *Swift-XRT* data are presented in Table 6. The photoelectric absorption model tbabs, with a neutral hydrogen column density fixed to its Galactic value (1.63×10^{20} cm^{-2}) was included in all fits. To account for the cross-calibration between *NuSTAR*-FPMA, *NuSTAR*-FPMB, and *Swift-XRT* a constant factor was included in the model, frozen at 1 for the FPMA spectra and free to vary for the FPMB and *XRT* spectra. The X-ray spectrum of the source is not well fitted by a simple PL model in both the observations (χ^2/d.o.f. = 1013/943 and 983/851, for the first and second observation, respectively), while a broken PL model yielded a good fit (χ^2/d.o.f. = 924/941 and 834/849). The result of fitting a broken PL to the spectrum collected on 2013 December 16–17 is shown in Fig. 4. In this model, the PL breaks from a slope of $\Gamma_1 = 0.97^{+0.09}_{-0.07}$ ($\Gamma_1 = 0.97^{+0.09}_{-0.07}$) below $E_{\text{break}} = 2.60^{+0.46}_{-0.56}$ keV ($2.98^{+0.47}_{-0.36}$ keV) to $\Gamma_2 = 1.37 \pm 0.01$ ($\Gamma_2 = 1.46 \pm 0.01$) for the first (second) observation (Table 6). The difference of the cross-calibration for the FPMB spectra with respect to FPMA spectra is 1–3 per cent, while for the *XRT* spectra is less than 10 per cent. These differences become larger (10–30 per cent) when a single PL model is used. By applying an F-test, the improvement of the fit with a broken PL is significant with respect to a single PL, with a probability that the null hypothesis is true of 1.6×10^{-19} and 5×10^{-31} for the first and second observation, respectively. These results are in agreement with those reported in Tagliaferri et al. (2015). By adding an extra absorption component at the redshift of the source (ztbabs) to the single PL,

the model provides a good fit to the spectrum, with an equivalent hydrogen column density of $\sim 10^{22}$ cm^{-2}, but the quality of the fit is worse than the broken PL model in both spectra (χ^2/d.o.f. = 966/942 and 895/850; Table 6). Sambruna et al. (2007) reported an equivalent hydrogen column density obtained by the fit of *Swift XRT* and *BAT* spectra of $0.25^{+0.34}_{-0.25} \times 10^{22}$ cm^{-2}, that is lower than the values obtained by fitting the *Swift-XRT* and *NuSTAR* spectra, but their statistics was significantly lower than that presented here.

6 DISCUSSION

6.1 γ-ray properties

PKS 2149−306 was not associated with a γ-ray source, either in the *LAT* bright source list obtained after three months of *Fermi* operation (Abdo et al. 2009) or in the First *Fermi LAT* source catalogue (Abdo et al. 2010a), indicating that its γ-ray activity was low during the first year of *Fermi* operation. On the other hand, this FSRQ is associated with 2FGL J2151.5−3021 and 3FGL J2151.8−3025 in the Second and Third *Fermi LAT* source catalogues (Nolan et al. 2012; Acero et al. 2015). The source is not included in the First *Fermi LAT* Catalog of Sources above 10 GeV (Ackermann et al. 2013). During the period 2008 August 4–2014 August 4, the γ-ray spectrum of PKS 2149−306 shows significant curvature, well described by an LP model with a spectral slope $\alpha = 2.36 \pm 0.05$, a curvature parameter around the peak $\beta = 0.29 \pm 0.03$, and an average flux of $(9.7 \pm 0.4) \times 10^{-8}$ ph cm^{-2} s^{-1}.

The source showed a significant increase in its γ-ray flux in 2011 February, and subsequently a strong γ-ray flare occurred in 2013 January (D'Ammando & Orienti 2012). The flux in 2013 January is about a factor of 8 higher than the average flux estimated over 6 yr of *Fermi* observations, with a significant change of the spectral slope ($\alpha = 1.99 \pm 0.11$) but a similar curvature parameter ($\beta = 0.28 \pm 0.06$). This suggests a shift of the IC peak to higher energies during this flaring activity. In contrast, no significant spectral changes were observed during the flaring activity in 2011 February, when the flux was about a factor of 5 higher than the average flux. In both flaring episodes the γ-ray spectrum is well described by an LP model. Considering the extragalactic background light (EBL) model discussed in Finke, Razzaque & Dermer (2010), at the redshift of PKS 2149−306 the optical depth should be $\tau \sim 1$ for 50 GeV photons. The maximum photon energy observed from the source during the 2013 flare is 4.8 GeV and is consistent with the current EBL models.

Thirteen FSRQ with $z > 2$ have been detected by *Fermi-LAT* during a γ-ray flare up to now. A significant increase of the flux together with a spectral evolution in γ rays was observed for the high-redshift FSRQ TXS 0536+145 (Orienti et al. 2014) and S5 0836+710 (Akyuz et al. 2013). In contrast, no significant spectral hardening was observed during the γ-ray flares for the high-redshift gravitationally lensed blazar PKS 1830−211 (Abdo et al. 2015).

During the 2013 flaring activity of PKS 2149−306, significant flux variation by a factor of 2 or more is clearly visible on 12-h and 6-h time-scales, with the peak of the flare resolved with 6-h binning. In particular, between the last 6-h bin of January 19 (MJD 56311.875) and the second 6-h bin of January 20 (MJD 56312.625), the flux increases from $F_1 = (88 \pm 40) \times 10^{-8}$ to $F_2 = (385 \pm 64) \times 10^{-8}$ ph cm^{-2} s^{-1} within $\Delta t = 12$ h, giving a flux doubling time-scale of $\tau_d = \Delta t \times \ln 2/\ln(F_2/F_1) \simeq 5.6$ h, and an exponential growth time-scale of $\tau_d/\ln2 \simeq 8$ h.

The event horizon light crossing time of a supermassive black hole (SMBH) is $t_{lc} \sim r_g/c = G\,M_9/c^3 \sim 1.4 \times M_9$ h, where r_g is

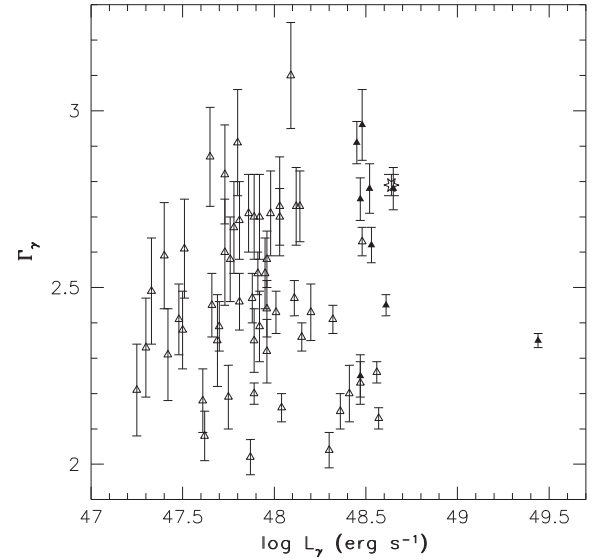**Figure 5.** γ-ray photon index versus apparent isotropic luminosity in the 0.1–100 GeV energy range for the blazars with $z > 2$ included in the 3FGL. The filled and open triangles represent the objects detected and not detected by *Swift-BAT*, respectively. The star represents PKS 2149−306.

the gravitational radius, $M_9 = (M/10^9)$ M$_\odot$ is the black hole (BH) mass, and c the speed of light (e.g. Begelman, Fabian & Rees 2008). In the case of PKS 2149−306, with a BH mass of 3.5×10^9 M$_\odot$ (Tagliaferri et al. 2015), we obtain a t_{lc} of $\sim$5 h, compatible with the minimum variability detected in the *LAT* light curve during 2013 January. This short time variability observed in γ rays constrains the size of the emitting region to $R < ct_{var}\delta/(1 + z) = 2.7 \times 10^{15}$ cm (assuming $\delta = 14$; Tagliaferri et al. 2015). This small size of the emitting region should correspond to a small distance from the central BH, putting the emitting region inside the broad-line region (BLR). This extremely small size is rather difficult to accommodate in the 'far dissipation' scenario (e.g. Tavecchio et al. 2010), where the external Compton scattering off the infrared photons from the torus is the main component that produces the high-energy emission, at least during flaring activity. This is not in contrast to the SED modelling of PKS 2149−306 presented in Tagliaferri et al. (2015), where low γ-ray activity contemporaneous to the *NuSTAR* observations was considered. In fact, different activity states of the same source may have different γ-ray emitting region locations. In the case of the 2011 February flare the statistics are not good enough to determine the flare shape.

High-redshift blazars tend to be the most luminous AGN due to their preferential selection by the *LAT* caused by Malmquist bias (Ackermann et al. 2015). The daily peak flux observed on 2013 January 20 is $(301 \pm 36) \times 10^{-8}$ ph cm^{-2} s^{-1}, corresponding to an apparent isotropic γ-ray luminosity of $(1.5 \pm 0.2) \times 10^{50}$ erg s^{-1}. On a 6-h time-scale, the flux reached a peak of $(385 \pm 70) \times 10^{-8}$ ph cm^{-2} s^{-1}, corresponding to an apparent isotropic γ-ray luminosity of $(1.9 \pm 0.3) \times 10^{50}$ erg s^{-1}. As a comparison, the average γ-ray luminosity over 6 yr of *Fermi* operation is 4.4×10^{48} erg s^{-1}. The peak values are comparable to the highest luminosity observed from FSRQ so far (i.e. 3C 454.3 and PKS 1830−211; Ackermann et al. 2010; Abdo et al. 2015) and a factor of two higher than the peak luminosity observed from TXS 0536+135, that is the most distant γ-ray flaring blazar observed by *Fermi-LAT* up to now (Orienti et al. 2014). In Fig. 5, we compare this value with the γ-ray luminosity of all blazars with $z > 2$ included in the 3FGL. We consider the
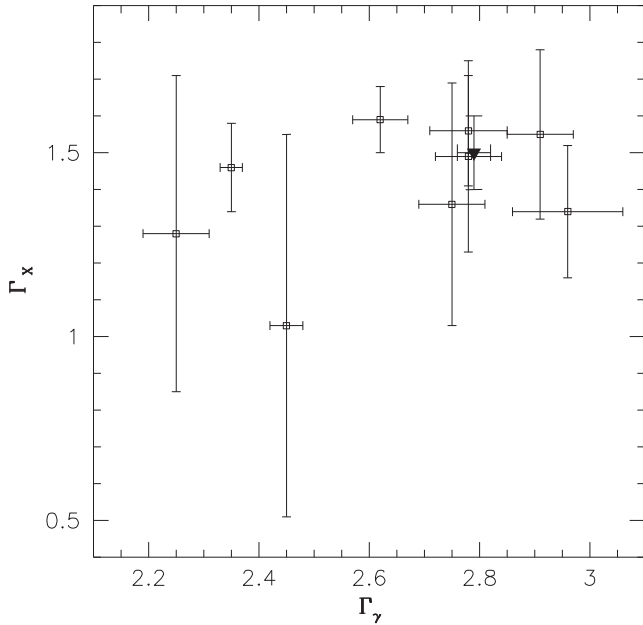
Figure 6. X-ray photon index from *Swift-BAT* versus γ-ray photon index from *Fermi-LAT* of the 10 high-redshift blazars detected by both instruments. The filled upside down triangle represents PKS 2149−306.

Figure 7. X-ray photon index versus 0.3–10 keV flux of PKS 2149−306 during 2001–2014. Filled circles are *Swift-XRT* observations; the open triangle represents the *XMM–Newton* observation.

high-redshift blazars detected also by *Swift-BAT* in hard X-rays. In particular, in the 70-month *Swift-BAT* catalogue (Baumgartner et al. 2013) there are 17 blazars with redshift $z > 2$. The filled and open triangles in Fig. 5 represent the blazars detected and not detected by *Swift-BAT*, respectively. The γ-ray luminosity, L_γ, is computed following Ghisellini, Maraschi & Tavecchio (2009):

$$L_\gamma = 4\pi d_L^2 \frac{S_\gamma}{(1+z)^{2-\Gamma_\gamma}} \qquad (1)$$

where S_γ is the energy flux between 100 MeV and 100 GeV, and Γ_γ is the photon index.

All these high-redshift blazars are FSRQ, with the exception of SDSS J145059.99+520111.7, PMN J0124-0624, MG4 J000800+4712, and PKS 0437-454 classified as BL Lac objects. Considering the average luminosity, PKS 2149−306 is the third brightest object among the high-redshift blazars detected by *LAT*, after PKS 1830−211 and PKS 0537−286.

By considering the blazars in the *Swift-BAT* catalogue, we note that all the high-redshift blazars detected by both *Fermi-LAT* and *Swift-BAT* have $L_\gamma > 2 \times 10^{48}$ erg s^{-1}, suggesting that only the most luminous γ-ray blazars are detected by both instruments. Most of the *LAT* sources detected by *BAT*, including PKS 2149−306, have a soft γ-ray photon index $\Gamma_\gamma > 2.5$. This corresponds in hard X-rays to a photon index $\Gamma_X < 1.6$ (see Fig. 6). This result confirms that the detection of these high-redshift blazars strongly depends on the position of their IC peaks. According to the blazar sequence (Fossati et al. 1998), as the bolometric luminosity of a blazar increases the synchrotron and IC peak moves to lower frequencies. Considering that high-redshift FSRQ are powerful blazars with high bolometric luminosity, their IC peak is usually expected in the 1–10 MeV energy range, below the energy range covered by *Fermi-LAT* (see e.g. Tagliaferri et al. 2015). However, during strong flaring activity the IC peak may shift to higher energies as in the case of the 2013 flare from PKS 2149−306.

28 high-redshift blazars detected by *Fermi-LAT* have $L_\gamma > 10^{48}$ erg s^{-1}. The vast majority of them have a BH mass $> 10^9$ M$_\odot$
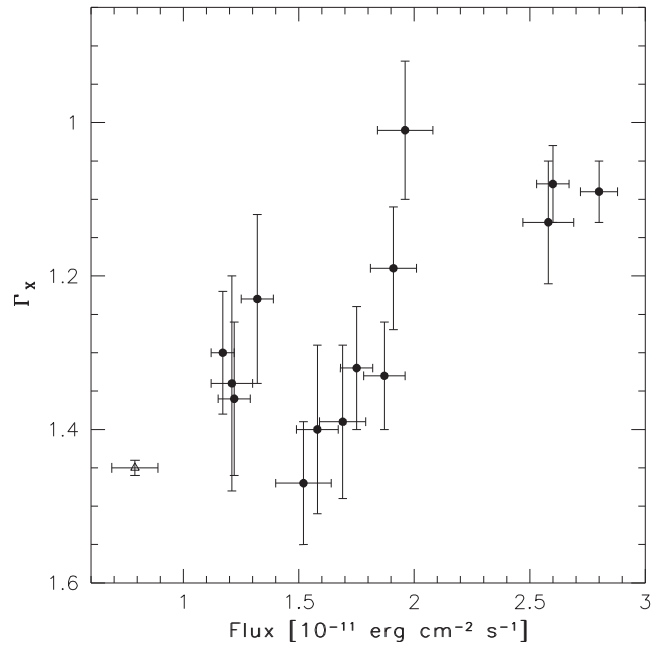
(Ghisellini et al. 2009, 2010, 2011, 2014b), confirming that the most powerful blazars have the heaviest BH (Ghisellini et al. 2013). In particular, PKS 2149−306 has a BH mass of 3.5×10^9 M$_\odot$, as estimated by Tagliaferri et al. (2015).

6.2 X-ray properties

We investigated the X-ray properties of PKS 2149−306 by means of *Swift-XRT*, *XMM–Newton*, and *NuSTAR* observations. The X-ray spectrum collected by *XMM–Newton* in 2001 is quite well modelled by a simple PL with a photon index of $\Gamma_X = 1.45 \pm 0.01$ and a 0.3–10 keV flux of 7.9×10^{-12} erg cm^{-2} s^{-1}. During 2005 December–2014 April, *Swift-XRT* observed the source with a 0.3–10 keV flux in the range $(1.2–2.8) \times 10^{-11}$ erg cm^{-2} s^{-1}, with a photon index varying between 1.0 and 1.5. Fig. 7 shows the X-ray photon index estimated from *Swift-XRT* and *XMM–Newton* observations as a function of the X-ray flux in the 0.3–10 keV range: despite the large errors, a hint of hardening of the spectrum with the increase of the flux is observed.

Unfortunately the *Swift* observations did not cover the γ-ray flaring periods detected in 2011 February and 2013 January, preventing us from investigating the X-ray behaviour during these γ-ray flaring events.

The *NuSTAR* spectra collected in the 3–76 keV energy range during 2013 December 17 and 2014 April 18 are well fitted by a simple PL with photon index $\Gamma_X = 1.37 \pm 0.01$ and $\Gamma_X = 1.46 \pm 0.01$, respectively. The two simultaneous observations of PKS 2149−306 by *Swift-XRT* and *NuSTAR* showed that the broad-band X-ray spectrum is well described by a broken PL model, with a very hard spectrum ($\Gamma_1 \sim 1$) below the break energy, at $E_{break} = 2.5–3.0$ keV, and $\Gamma_2 = 1.37 \pm 0.01$ and 1.46 ± 0.01 above the break energy. *Swift-BAT* and *BeppoSAX* observed a photon index $\Gamma_X = 1.50 \pm 0.10$ (Baumgartner et al. 2013) and $\Gamma_X = 1.40 \pm 0.04$ (Elvis et al. 2000) in the 14–195 keV and 20–200 keV energy range,

respectively, in agreement with the photon index Γ_2 obtained by the two *Swift-XRT* and *NuSTAR* joint fits. The 3–76 keV flux varied by about 40 per cent between the first and second *NuSTAR* observation. At the same time the 0.3–10 keV flux varied by less than 10 per cent. In the same way, the photon index below the break energy did not change, while the photon index above the break energy was harder when the source was brighter.

In several high-redshift ($z > 4$) blazars a steepening of the soft X-ray spectrum has been observed (e.g. Yuan et al. 2006, and references therein). This steepening may be due to either an excess of absorption in the soft X-ray part of the spectrum or due to an intrinsic curvature of the electron energy distribution responsible for the X-ray emission. In PKS 2149−306 this feature was observed below 3 keV, and an improvement of the fit is observed when an extra absorber at the redshift of the source ($N_H^z \sim 10^{22}$ cm^{-2}) is added to the simple PL model. However, this improvement is not as good as when we use a broken PL model. The AGN may be surrounded by a dense plasma in form of a wind or an outflow (e.g. Fabian 1999). This intervening material may be responsible for the extra absorption observed in high-redshift quasars (e.g. Vignali et al. 2005). However, in contrast to radio-loud quasars, it is unlikely that for a blazar like PKS 2149−306 such a large gas column density in the line of sight is not removed by the relativistic jet that should be well aligned with the line of sight. Moreover, with a hydrogen column density of about 10^{22} cm^{-2} obtained by fitting the X-ray spectrum the corresponding optical obscuration (see e.g. Guver & Ozel 2009) would be very high ($A_V \sim 10$) and the source would not be detectable in optical–UV with the short exposures of the *Swift* observations. This problem may be solved by invoking a high-ionization state of the gas, but it is not possible to have conclusive evidence from its X-ray spectrum. In fact, due to the redshift of this source the most important spectral features used as a diagnostic are out of the energy range covered by *Swift* and *XMM–Newton*.

The most likely explanation of the steepening of the spectrum is that the soft X-ray emission is produced by external Compton radiation from the electrons at the lower end of the energy distribution (e.g. Tavecchio et al. 2007). This is in agreement with the stable photon index below 3 keV and the change of the photon index above $\sim$3 keV, where the emission is produced by the most energetic electrons. In this context the lack of a clear steepening in the X-ray spectrum collected by *XMM–Newton* in 2001 may be related to the lower flux with respect to that estimated during the *Swift-XRT* and *NuSTAR* observations. The intrinsic curvature in soft X-rays would be less evident during the low activity of the source. The situation may be more complex due to the possible presence in the X-ray band also of the synchrotron self-Compton emission (SSC). However, the relative importance of the SSC component should decrease with the luminosity of the source (e.g. Ghisellini et al. 1998), and therefore should be negligible in powerful FSRQ such as PKS 2149−306. Moreover, Celotti et al. (2007) proposed the presence of a spectral component in X-rays produced by the Comptonization of ambient photons by cold electrons in the jet approaching the BLR. However, the direct detection of such a component has remained elusive. It is worth nothing that the broad-band spectrum of PKS 2149−306 including the *Swift-XRT* and *NuSTAR* data are better fitted by considering the emitting region outside the BLR (e.g. Tagliaferri et al. 2015), where the contribution of the bulk Comptonization should be negligible.

Considering the blazars included in the 70-month *Swift BAT* catalogue with a redshift $z > 2$, 7 out of 17 have not been detected by *Fermi-LAT* so far. Only sources with a $\Gamma_X < 1.6$ have been detected in γ rays, while no dependence on the X-ray luminosity seems to be
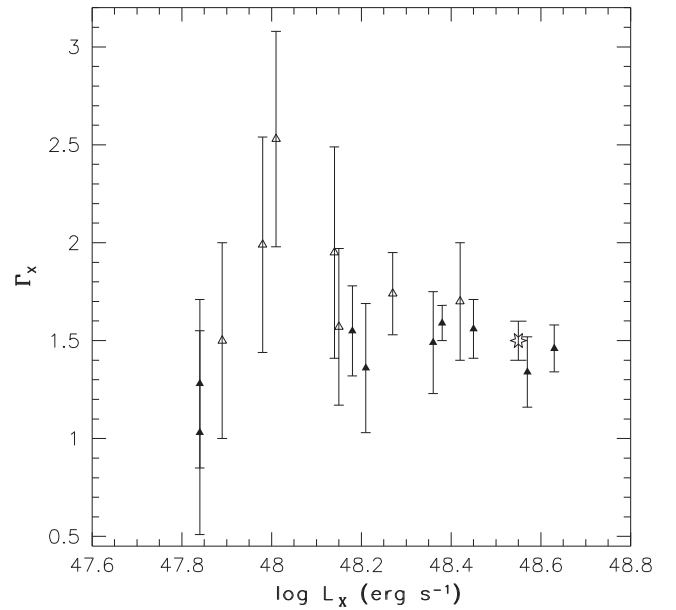

Figure 8. X-ray photon index versus X-ray apparent isotropic luminosity in the 14–195 keV energy range for the blazars with $z > 2$ detected by *Swift-BAT*. The filled and open triangles represent the objects detected and not detected by *Fermi-LAT*, respectively. The star represents PKS 2149−306.

evident (Fig. 8). This is confirmed by the fact that the average photon index of the FSRQ detected by *LAT*, $< \Gamma_X^{\mathrm{LAT}} > = 1.42 \pm 0.09$ is quite different from that of the sources detected by *BAT* and not by *LAT*, $< \Gamma_X^{\mathrm{no-LAT}} > = 1.85 \pm 0.17$. Seven blazars with $z > 3$ have been detected by *Swift-BAT*, and another one, IGR J12319−0749, by *INTEGRAL*-IBIS (Bassani et al. 2012). In addition, two blazars at redshift $z > 5$ have been detected by *NuSTAR*. Only two of these ten blazars have been detected by *Fermi-LAT*: PKS 0537−286 (e.g. Bottacini et al. 2010) and TXS 0800+618 (e.g. Ghisellini et al. 2010), confirming that the γ-ray energy range is not ideal for detecting blazars at redshift >3. Among the FSRQ detected by both *BAT* and *LAT*, PKS 2149−306 is the third most luminous after PKS 1830−211 (e.g. Abdo et al. 2015) and B2 0743+25 (e.g. Ghisellini et al. 2010).

6.3 Optical and UV properties

In powerful high-redshift blazars, such as PKS 2149−306, the synchrotron peak is shifted to the mm-regime, leaving the thermal emission from the accretion disc as the dominant contribution in the optical–UV part of the spectrum (e.g. Tagliaferri et al. 2015). This accretion disc emission is not expected to vary on short time-scales. During 2005–2014, the difference between the maximum and minimum magnitude observed by *Swift-UVOT* is 0.6, 0.7, 1.1, 0.8, 0.6, and 0.6 mag (corresponding to a variation of the flux density of 1.5, 1.8, 2.8, 2, 1.5, 1.5) from the v to the $w2$ band. No significant variability was observed on a time-scale of a few days, in agreement with thermal emission from an accretion disc.

7 SUMMARY

In this paper, we discussed the γ-ray and X-ray properties of the high-redshift FSRQ PKS 2149−306 by means of *Fermi-LAT*, *NuSTAR*, *XMM–Newton*, and *Swift* data. We summarize our main conclusions as follows.

(i) PKS 2149−306 showed a significant increase in its γ-ray activity in 2011 February and 2013 January. During the 2013 flare the flux increase was accompanied by a significant change of the spectral slope, not observed during the 2011 flare.

(ii) During the 2013 γ-ray flaring activity significant flux variations are observed on a 6-h time-scale, compatible with the light crossing time of the event horizon of the SMBH. On 2013 January 20, the source reached a daily γ-ray peak flux of $(301 \pm 36) \times 10^{-8}$ ph cm^{-2} s^{-1}, up to $(385 \pm 70) \times 10^{-8}$ ph cm^{-2} s^{-1} on a 6-h time-scale. These values correspond to an apparent isotropic γ-ray luminosity of $(1.5 \pm 0.2) \times 10^{50}$ and $(1.9 \pm 0.3) \times 10^{50}$ erg s^{-1}, respectively, comparable to the highest values observed from FSRQ up to now.

(iii) The average γ-ray luminosity of PKS 2149−306 over 6 yr of *Fermi* operation is 4.4×10^{48} erg s^{-1}. This is the third brightest blazar with $z > 2$ detected by *LAT*, after PKS 1830−211 and PKS 0537−286.

(iv) All high-redshift blazars detected by both *Fermi-LAT* and *Swift-BAT* have an $L_\gamma > 2 \times 10^{48}$ erg s^{-1}, suggesting that only the most luminous γ-ray blazars are detected by both instruments. Like most of the *LAT* blazars detected by *BAT*, PKS 2149−306 has a soft γ-ray photon index $\Gamma_\gamma > 2.5$. This corresponds to a photon index $\Gamma_X < 1.6$ in hard X-rays.

(v) Among the FSRQ with $z > 2$ detected by both *BAT* and *LAT*, PKS 2149−306 is the third most luminous in hard X-rays after PKS 1830−211 and B2 0743+25.

(vi) The broad-band X-ray spectrum of PKS 2149−306 observed by *Swift-XRT* and *NuSTAR* is well described by a broken PL model, with a very hard spectrum ($\Gamma_1 \sim 1$) below the break energy, at $E_{break} = 2.5$–3.0 keV, and $\Gamma_2 \sim 1.4$–1.5 above the break energy.

(vii) The steepening of the spectrum below ~ 3 keV could be due to the fact that the soft X-ray emission is produced by the low-energy tail of the relativistic electrons producing IC emission. This is in agreement with the small variability amplitude and the lack of spectral changes observed in that part of the X-ray spectrum between the two *NuSTAR* and *Swift* joint observations. An extra absorption due to material surrounding the SMBH is unlikely because the relativistic jet should efficiently remove the gas along the line of sight. Moreover, this extra absorption should correspond to a very large extinction in optical and UV, in contrast to the detection of the source by *Swift-UVOT*.

(viii) *Fermi-LAT* and *Swift-BAT* observations are confirming that the hard X-ray band is more effective in selecting bright FSRQ at $z > 3$ (see e.g. Ghisellini et al. 2010; Ajello et al. 2012), while the γ-ray band is very effective up to $z = 2$ (see e.g. Ackermann et al. 2015).

Further multiwavelength observations of PKS 2149−306 will be important for shedding light on the properties of high−z blazars. In particular, simultaneous optical-to-X-ray observations during a γ-ray flaring activity will allow us to compare its broad-band spectral energy distribution during both low and high activity states, constraining the emission mechanisms at work.

ACKNOWLEDGEMENTS

REFERENCES

Abdo A. A. et al., 2009, ApJ, 707, L142
Abdo A. A. et al., 2010a, ApJS, 188, 405
Abdo A. A. et al., 2010b, ApJ, 721, 1425
Abdo A. A. et al., 2015, ApJ, 799, 143
Acero F. et al., 2015, ApJS, 218, 23
Ackermann M. et al., 2010, ApJ, 721, 1383
Ackermann M. et al., 2012, ApJ, 747, 104
Ackermann M. et al., 2013, ApJS, 209, 34
Ackermann M. et al., 2015, ApJS, 810, 14
Ajello M., Alexander D. M., Greiner J., Madejski G. M., Gehrels N., Burlon D., 2012, ApJ, 749, 21
Akyuz A. et al., 2013, A&A, 556, A71
Atwood W. B. et al., 2009, ApJ, 697, 1071
Barthelmy S. D. et al., 2005, Space Ssci. Rev., 120, 143
Bassani L. et al., 2012, A&A, 543, A1
Baumgartner W. H., Tueller J., Markwardt C. B., Skinner G. K., Barthelmy S., Mushotzky R. F., Evans P. A., Gehrels N., 2013, ApJS, 207, 19
Beckmann V. et al., 2009, A&A, 505, 417
Begelman M. C., Fabian A. C., Rees J. M., 2008, MNRAS, 384, L19
Bianchin V. et al., 2009, A&A, 496, 423
Bottacini E. et al., 2010, A&A, 509, 69
Burrows D. N. et al., 2005, Space Sci. Rev., 120, 165
Cappi M., Matsuoka M., Comastri A., Brinkmann W., Elvis M., Palumbo G. G. C., Vignali C., 1997, ApJ, 478, 492
Celotti A., Ghisellini G., Fabian A. C., 2007, MNRAS, 375, 417
D'Ammando F., Orienti M., 2012, Astron. Telegram, 4706
Elvis M., Fiore F., Siemiginowska A., Bechtold J., Mathur S., McDowell J., 2000, ApJ, 543, 545
Fabian A. C., 1999, MNRAS, 308, L39
Fang T., Marshall H. L., Bryan G. L., Canizares C. R., 2001, ApJ, 555, 356
Ferrero E., Brinkmann E., 2003, A&A, 402, 465
Finke J. D., Razzaque S., Dermer C. D., 2010, ApJ, 712, 238
Fossati G., Maraschi L., Celotti A., Comastri A., Ghisellini G., 1998, MNRAS, 299, 433
Gehrels N. et al., 2004, ApJ, 611, 1005
Ghisellini G., 2013, Mem. Soc. Astron. Ital., 84, 719
Ghisellini G., Celotti A., Fossati G., Maraschi L., Comastri A., 1998, MNRAS, 301, 451
Ghisellini G., Maraschi L., Tavecchio F., 2009, MNRAS, 396, L105
Ghisellini G. et al., 2010, MNRAS, 405, 387
Ghisellini G. et al., 2011, MNRAS, 411, 901

Ghisellini G., Haardt F., Della Ceca R., Volonteri M., Sbarrato T., 2013, MNRAS, 432, 2818

Ghisellini G., Sbarrato T., Tagliaferri G., Foschini L., Tavecchio F., Ghirlanda G., Braito V., Gehrels N., 2014a, MNRAS, 440, L111

Ghisellini G., Tavecchio F., Maraschi L., Celotti A., Sbarrato T., 2014b, Nature, 515, 376

Guver T., Ozel F., 2009, MNRAS, 400, 2050

Harrison F. A. et al., 2013, ApJ, 770, 103

Jansen F. et al., 2001, A&A, 365, L1

Johnston K. J. et al., 1995, AJ, 110, 880

Kalberla P. M. W., Burton W. B., Hartmann D., Arnal E. M., Bajaja E., Morras R., Pöppel W. G. L., 2005, A&A, 440, 775

Komatsu E. et al., 2011, ApJS, 192, 18

Mattox J. R. et al., 1996, ApJ, 461, 396

Nolan P. et al., 2012, ApJS, 199, 31

Orienti M., D'Ammando F., Giroletti M., Finke J., Ajello M., Dallacasa D., Venturi T., 2014, MNRAS, 444, 3040

Page K. L., O'Brien P. T., Reeves J. N., Turner M. J. L., 2004, MNRAS, 347, 316

Romani R. W., 2006, AJ, 132, 1959

Romani R. W., Sowards-Emmerd D., Greenhill L., Michelson P., 2004, ApJ, 610, L9

Roming P. W. A. et al., 2005, Space Sci. Rev., 120, 95

Sambruna R. M., Tavecchio F., Ghisellini G., Donato D., Holland S. T., Markwardt C. B., Tueller J., Mushotzky R. F., 2007, ApJ, 669, 884

Sbarrato T. et al., 2013, ApJ, 777, 147

Siebert J., Matsuoka M., Brinkmann W., Cappi M., Mihara T., Takahashi T., 1996, A&A, 307, 8

Tagliaferri G. et al., 2015, ApJ, 807, 167

Tavecchio F., Maraschi L., Ghisellini G., Kataoka J., Foschini L., Sambruna R. M., Tagliaferri G., 2007, ApJ, 665, 980

Tavecchio F., Ghisellini G., Bonnoli G., Ghirlanda G., 2010, MNRAS, 405, L94

Vignali C., Brandt W. N., Schneider D. P., Kaspi S., 2005, AJ, 129, 2519

Wilkes B. J., 1986, MNRAS, 218, 331

Wilms J., Allen A., McCray R., 2000, ApJ, 542, 914

Yaqoob T., George I. M., Nandra K., Turner T. J., Zobair S., Serlemitsos P. J., 1999, ApJ, 525, L9

Yuan W., Fabian A. C., Worsley M. A., McMahon R. G., 2006, MNRAS, 368, 985

This paper has been typeset from a TEX/LATEX file prepared by the author.